Computer-Aided Design for Additive Manufacturing of Cellular Structures

David W. Rosen

Georgia Institute of Technology, david.rosen@me.gatech.edu

ABSTRACT

Additive Manufacturing (AM) technologies, informally called "rapid prototyping," enable the fabrication of parts and devices that are geometrically complex, have graded material compositions, and can be customized. In this paper, we focus on cellular materials and structures, which can lead to designs that are very geometrically complex. In order to take advantage of AM capabilities, new design and CAD methods must be developed. Two advances are reported in this paper. First, a new Design for Additive Manufacturing (DFAM) method is proposed that supports part and specification modeling, process planning, and manufacturing simulations. The method is based on the process-structure-property-behavior model that is common in the materials design literature. Second, Manufacturable ELements (MELs) are proposed as an intermediate representation for supporting the manufacturing related aspects of the method. These MELs represent process planning information for discrete geometric regions of a part and also enable process simulation. An example of a cover plate with over 14,000 shape features is used to illustrate the DFAM method and design-manufacturing integration achievable with MELs.

Keywords: Additive Manufacturing, Rapid Prototyping, Design for Manufacture, Cellular Structures.

1. INTRODUCTION

1.1 Design for Additive Manufacturing

Design for manufacturing (DFM) has typically meant that designers should tailor their designs to eliminate manufacturing difficulties and minimize costs. However, the improvement of rapid prototyping, or Additive Manufacturing (AM), technologies provides an opportunity to re-think DFM to take advantage of the unique capabilities of these technologies. Several companies are now using AM technologies for production manufacturing. For example, Siemens, Phonak, Widex, and the other hearing aid manufacturers use selective laser sintering and stereolithography (SL) machines to produce hearing aid shells, Align Technology uses stereolithography to fabricate molds for producing clear braces ("aligners"), and Boeing and its suppliers use selective laser sintering to produce ducts and similar parts for F-18 fighter jets. In the first three cases, AM machines enable one-off, custom manufacturing of 10's to 100's of thousands of parts. In the last case, AM technology enables low volume manufacturing and, at least as importantly, piece part reductions to greatly simplify product assembly. More generally, the unique capabilities of AM technologies enable new opportunities for customization, very significant improvements in product performance, multi-functionality, and lower overall manufacturing costs. These unique capabilities include:

- **Shape complexity:** it is possible to build virtually any shape, lot sizes of one are practical, customized geometries are achieved readily, and shape optimization is enabled.
- **Material complexity:** material can be processed one point, or one layer, at a time, enabling the manufacture of parts with complex material compositions and designed property gradients.
- **Hierarchical complexity:** hierarchical multi-scale structures can be designed and fabricated from the microstructure through geometric mesostructure (sizes in the millimeter range) to the part-scale macrostructure.

New CAD and DFM methods are needed in order to take advantage of these capabilities. In the hearing aid and aligner cases, new CAD systems had to be developed to enable efficient shape modeling and part design. During a U.S. government sponsored study of European researcher groups [11], many researchers said that they foresaw the lack of capable CAD tools as a serious impediment for their research and for the utilization of AM technologies for production manufacturing applications. However, if suitable CAD and DFM methods and tools can be developed, designers can design devices with significantly improved performance that fully utilize material, and with efficient manufacturing processes. With the shape, material, and hierarchical complexity capabilities, DFM can move from an

emphasis on cost minimization to a focus on achieving heretofore unrealizable capabilities. Hence, a new definition of DFM can be proposed. DFM for Additive Manufacturing (DFAM) is the:

> Synthesis of shapes, sizes, geometric mesostructures, and material compositions and microstructures to best utilize manufacturing process capabilities to achieve desired performance and other life-cycle objectives.

In order to achieve this new concept of DFAM and enable wide ranges of new applications, new approaches, methods, and tools are needed. The focus in this paper is on the application of cellular materials to replace bulk materials. Cellular materials provide many more design variables, but with those variables comes more complexity. New design, analysis, and manufacturing technologies are needed as a result.

1.2 Cellular Materials

The concept of designed cellular materials is motivated by the desire to put material only where it is needed for a specific application. From a mechanical engineering viewpoint, a key advantage offered by cellular materials is high strength accompanied by a relatively low mass. These materials can provide good energy absorption characteristics and good thermal and acoustic insulation properties as well [4]. Cellular materials include foams, honeycombs, lattices, and similar constructions. When the characteristic lengths of the cells are in the range of 0.1 to 10 mm, we refer to these materials as mesostructured materials. Mesostructured materials that are not produced using stochastic processes (e.g. foaming) are called designed cellular materials. In this paper, we focus on designed lattice materials.

In the past 10 years, the area of lattice materials has received considerable attention due to their inherent advantages over foams in providing light, stiff, and strong materials [1]. Lattice structures tend to have geometry variations in three dimensions; some of our designs are shown in Figure 1. As pointed out in [2], the strength of foams scales as $\rho^{1.5}$, whereas lattice structure strength scales as ρ, where ρ is the volumetric density of the material. As a result, lattices with a $\rho = 0.1$ are about 3 times stronger than a typical foam. The strength differences lie in the nature of material deformation: the foam is governed by cell wall bending, while lattice elements stretch and compress. The examples in Fig. 1 utilize the octet-truss (shown on the left), but many other lattice structures have been developed and studied (e.g., kagome, Kelvin foam). We have developed methods for designing lattice mesostructure for parts [15] and have developed design-for-manufacturing rules for their fabrication in SL.

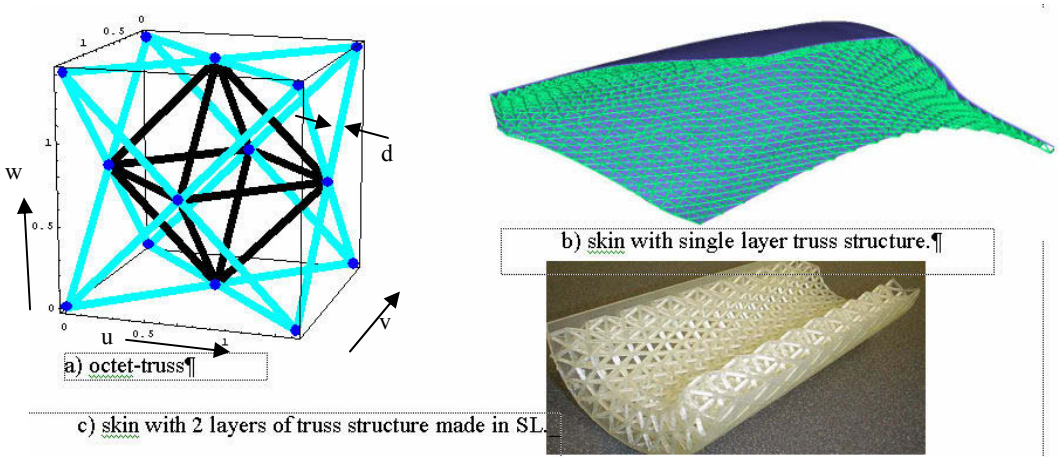

Fig. 1: Octet-truss unit cell and example parts with octet-truss mesostructures.

Methods of continuum mechanics have been applied to various mesostructured materials. Ashby and co-workers wrote a book on metal foam design and analysis [1]. They and others have applied similar methods to the analysis of lattice structures. The octet truss in Fig. 1 has been extensively analyzed. Deshpande et al. [4] treated the octet truss unit cell as a collection of tension-compression bars that are pin-jointed at vertices and derived analytical models of their collapse behavior for many combinations of stresses. Their results match finite element model behavior well, but tend to under-predict the strength and stiffness of octet trusses due to their assumption of pin-jointed vertices. Wang and McDowell [16] extended this study to include several other lattice cells. Recently, we have been developing a more general analytical model of lattice behavior [7]. From our general model, models for octet and other lattice structures can be derived. We base our model on a single vertex with a collection of struts incident on that vertex. This vertex model will be our base "unit cell" for representation and modeling purposes.

1.3 Requirements for DFAM

The concept of mesostructured materials is motivated by the desire to put material only where it is needed for a specific application. Achieving high stiffness or strength and minimal weight are typical objectives. Multifunctional requirements are also common, such as structural strength and vibration absorption. The area of compliant mechanisms shares the same motivation, where the local compliance of the structure enables the mechanism to perform specified motions.

We hypothesize that designed mesostructures will enable structures and mechanisms to be designed that perform better than parts with bulk or non-designed mesostructures, particularly for multifunctional applications. Testing this hypothesis requires the ability to bridge the meso to macro size scales. To do this, we need to first recognize some requirements on DFAM methods and CAD-DFAM tools that will be developed, with a related objective of utilizing the unique capabilities of AM technologies. The requirements that we propose include the capability to:

- R1: Represent and design with hundreds of thousands of shape elements, enabling large complex design problems as well as designed material mesostructures.
- R2: Represent complex material compositions and ensure that they are physically meaningful.
- R3: Determine mechanical properties from material compositions and mesostructures across length scales.
- R4: Ensure that specified shapes, material structures, and properties are manufacturable.
- R5: Ensure that as-manufactured designs achieve requirements.

In order to achieve these requirements, several new technologies are required. Our approach has five main elements (requirements that they address are appended):

- Implicit representations of shapes and specifications of desired distributions of materials and physical properties (e.g., density, refractive index, elastic modulus). Implicit representations are of two types, implicit modeling and non-manifold modeling of shape skeletons. With implicit modeling, evaluations of designs need only be decomposed to the resolution needed for the most detailed analysis. R1, R2, R3
- "Manufacturable Elements" (MEL's) that contain geometry, material, properties, and uncertainties in these quantities that are produced by elementary manufacturing operations. R2, R3, R4
- Inverse design methods for process planning that effectively and efficiently determine values of process variables from MEL representations of parts. R4
- Manufacturing simulations that are performed by composing MEL's according to their interaction rules, where composition is achieved by solving simultaneous implicit equations. R2, R3, R4, R5
- DFAM templates that enable formulation and solution of typical DFM problems. R4, R5

Each of these five new technologies is addressed, at least in part, in this paper. In the next section, the formal framework for our DFAM approach is presented, providing the larger context for this research. In Section 3, the technologies being developed for DFAM are presented, with an emphasis on the problem formulations and Manufacturing Elements. An example is presented in Section 4 that covers part design, manufacturability analysis, process planning, and process simulation. Conclusions are drawn in the final section.

2. FORMAL FRAMEWORK FOR DFAM

It is helpful to introduce a formal notation for the subsequent discussion. Let a solid model with material composition and other material-related attributes be denoted as $S = (G, M)$, where G is the solid geometric model and M is the attribute space, with some attributes being applied only to regions of G. S denotes the structure of the design. We will borrow the process-structure-property relationships framework from the materials science field to model a design [8]. The manufacturing process space, P, consists of process plans with sequences of operations and values of process variables. Property space T contains information about part properties that are derivable from S using physical principles; e.g., mechanical, thermal, and electrical properties. Finally, we will add behavior space, B, which contains information about a part's actual and desired behavior given some loading and boundary conditions. The relationships among these spaces are shown in Fig. 2.

Mappings are defined among these spaces. Mapping Φ represents a manufacturing analysis that determines material composition and microstructure, and possibly as-manufactured part shape from a process plan. Mapping Γ represents a material science analysis of a material, and possibly part geometry, to arrive at a set of mechanical and other properties. It is possible that this mapping can be determined once, then reused for different applications (not design- or part-specific). Some standard engineering tasks can be described using this notation.

$\Psi: (S,T) \rightarrow B$	Engineering analysis
$\Phi^{-1}: S \rightarrow P$	Process planning

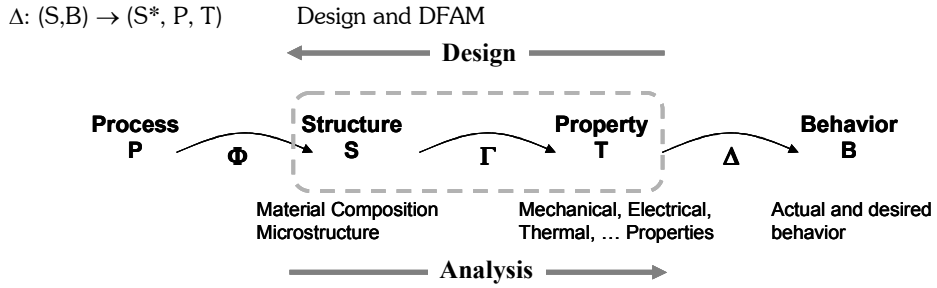

Fig. 2: Process-Structure-Property-Behavior Mappings.

The mappings shown in Fig. 2 capture important relationships among design attributes across several size scales. However, additional richness enables the multi-scale aspects of both geometric and material models to be captured. The process, structure, and property models will be divided into geometric and material models in order to emphasize their different decompositions. Fig. 3 shows the framework from Fig. 2 with separate Material and Geometry levels. As one moves from right to left, the relevant size scales decrease. Similarly, when one moves from top to bottom, smaller size scales become important. These levels and size scales will be further explained in the next section.

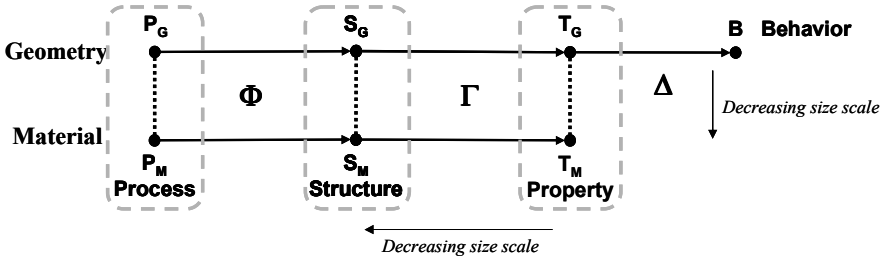

Fig. 3: Expanded CADfAM Framework with Geometry and Material Layers.

3. DFAM METHOD, SYSTEM, AND TECHNOLOGIES

3.1 DFAM Method and System

The overall DFAM method consists of a traversal of the frameworks in Figs. 2 and 3 from Behavior to Process, then back again to Behavior. The traversal from Behavior to Process can be called design, where functional requirements are mapped to properties and geometry that satisfy those requirements to structures and through process planning to arrive at a potential manufacturing process. Going in the reverse direction, one can simulate the designed device and its manufacturing process to determine how well it satisfies the original requirements.

Fig. 4 shows the proposed DFAM system that embodies the method outlined above. To the right in Fig. 4, the designer can define the DFAM synthesis problem, using an existing problem template if desired. For different problem types, different solution methods and algorithms will be available. Analysis codes, including FEA, boundary element, and specialty codes, will be integrated to determine design behavior. In the middle of Fig. 4, the heterogeneous solid modeler (HSM) is illustrated (heterogeneous denotes that material and other property information will be modeled). Libraries of materials and mesostructures enable rapid construction of design models. To the left, the manufacturing modules are shown. Both process planning and simulation modules will be included. After planning a manufacturing process, the idea is that the process will be simulated on the current design to determine the as-manufactured shapes, sizes, mesostructures, and microstructures. The as-manufactured model will then by analyzed to determine whether or not it actually meets design objectives.

At present, elements of all indicated modules have been developed. The CAD system itself is limited in that material composition and most property distributions cannot be modeled directly. Most modules have limitations and their integration is limited. However, enough of the system has been developed in order to illustrate the potential of the system and to conduct some example design problems with complex cellular structures, as will be seen in Section 4.

3.2 CAD = Structure + Property

The CAD system proposed here consists of the Structure and Property elements of Figs. 2 and 3. Our proposed geometric representation is a combination of implicit, non-manifold, and parametric modeling, with the capability of

generating BReps when needed. Implicit modeling is used to represent overall part geometry, while non-manifold modeling is used to represent shape skeletons. Parametric modeling is necessary when decomposing the overall part geometry into cellular structures; each cell type will be represented as a parametric model.

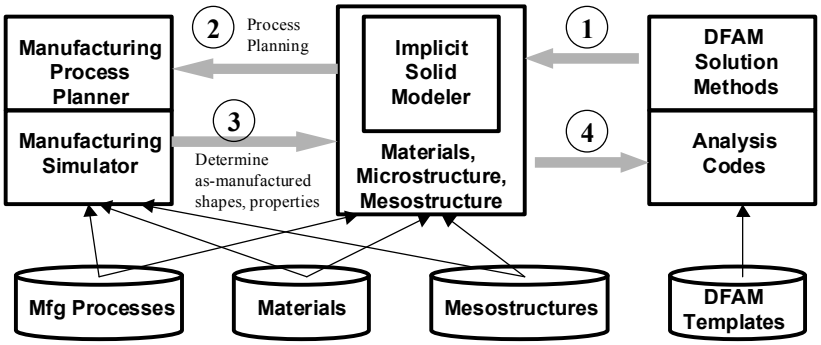

Fig. 4: DFAM System and Overall Method.

Implicit modeling has many advantages over conventional BRep, CSG, cellular decomposition, and hybrid approaches, including its conciseness, ability to model with any analytic surface models, and its avoidance of complex geometric and topological representations [3]. The primary disadvantage is that an explicit boundary representation is not maintained, making visualization and other evaluations more difficult than with some representation types. For HSM, additional advantages are apparent. Implicit modeling offers a unified approach for representing geometry, materials, and distributions of any physical quantity. A common solution method can be used to solve for material compositions, analysis results (e.g., deflections, stresses, temperatures), and for spatial decompositions if they can be modeled as boundary value problems [13]. Furthermore, it provides a method for decomposing geometry and other properties to arbitrary resolutions which is useful for generating visualizations and manufacturing process plans.

Cellular structures are represented parametrically. The octet lattice unit cell shown in Fig. 1 includes spatial parameters u, v, w and size parameter d for strut diameters. That is, one can think of a unit cell as a primitive that can be mapped into a trivariate volume. Such primitives can be used to fill (tile) a volume that is modeled as a trivariate Bezier or B-spline volume. The mapping $\Gamma^{-1}(\mathbf{T_G}) \rightarrow \mathbf{S_G}$ is a spatial decomposition of a volume into a collection of unit cells. The decompositions of interest here are essentially mapped hexahedral meshes, with each element of the mesh consisting of an appropriate unit cell. In this manner, lattice and other cellular structures can be generated readily.

Non-manifold modeling is used to represent shape skeletons. For lattice structures, it is often sufficient to represent struts as line segments terminated by nodes. Radius parameters are associated with struts and nodes to enable reasoning about the 3D geometry of lattices and enable generation of 3D solid models, analysis models, and manufacturing models. We use a simple non-manifold model based on that of Gursoz *et al*. [5], which is particularly useful when representing lattices with skins. Such models are represented by the centerlines of the lattice struts and the mid-plane of the skin (surface). Non-manifold capability enables the determination of which side of the skin the truss is on, among other reasoning tasks.

3.3 Manufacturable Elements

A Manufacturable ELement (MEL) is a predefined, parameterized decomposition of a volumetric region of a part. For the lattice structures under investigation in this paper, MEL definition is straightforward: scan patterns and scan variables are associated with each strut in a unit cell. Consider the octet unit cell in Fig. 1 and assume it is being built in a SL machine vertically upward. For each layer in the SL build process, the unit cell is sliced by a plane. For the vertical struts, the intersection of the plane and the strut is a circle. For slanted struts, the intersection is an ellipse, while for horizontal struts, the intersection is a rectangle. Each case can be handled readily.

The cases for vertical and slanted struts are shown in Fig. 5. The notation is as follows: r = strut radius, W_0 = laser beam radius, θ = strut angle, r_l = major axis of ellipse (with minor axis = r), and $p = (p_x, p_y)$ = center of intersected circle or ellipse. The specific parameters in the cases were determined empirically and give reasonable results for typical SL resins and laser scanning speeds. For example, case a) $r_l \leq 1.4\ W_0$ or $1.6\ W_0$ or other multiple of W_0 could have been selected and the laser irradiation time can be determined easily. However, long irradiation times can cause

cured struts to become too thick, while short irradiation times may not enable the layer to adhere to the previous one. The multiple 1.5 times W_0 is a reasonable compromise value. For horizontal struts, cases b), c), and d) apply.
Using the standard SL exposure model from Jacobs [6], the irradiation time for points and scan speeds for lines can be computed easily. For reasonably long scan vectors (more than ~3 times the laser beam diameter), the exposure received at a point (y, z) in the vat by a scan along the x axis is given by

$$E(x,y,z) = \sqrt{\frac{2}{\pi}} \frac{P_L}{W_0 V_s} e^{-2y^2/W_0^2} e^{-z/D_p} \tag{1}$$

where P_L = laser power [mW], V_s = scan speed [mm/s], and D_p = depth of penetration [mm] (taken to be a constant measure of a resin's sensitivity to laser energy). SL resins are assumed to be cured (form a solid) when they receive exposure that is equal to or greater than a certain amount, called the resin's critical exposure, E_c [mJ/mm^2]. For a layer thickness of l = 0.1 mm, it is typical to cure the resin to a depth of 0.15 mm, or 1.5 times the layer thickness. This cure depth reaches a maximum along a scan's centerline (when y = 0). Eqn. 1 can be rearranged to solve for V_s as follows in order to compute the scan velocity to give a cure depth of 1.5 times the layer thickness:

$$V_s = \sqrt{\frac{2}{\pi}} \frac{P_L}{W_0 E_c} e^{\left(-\frac{1.5l}{D_p}\right)} \tag{2}$$

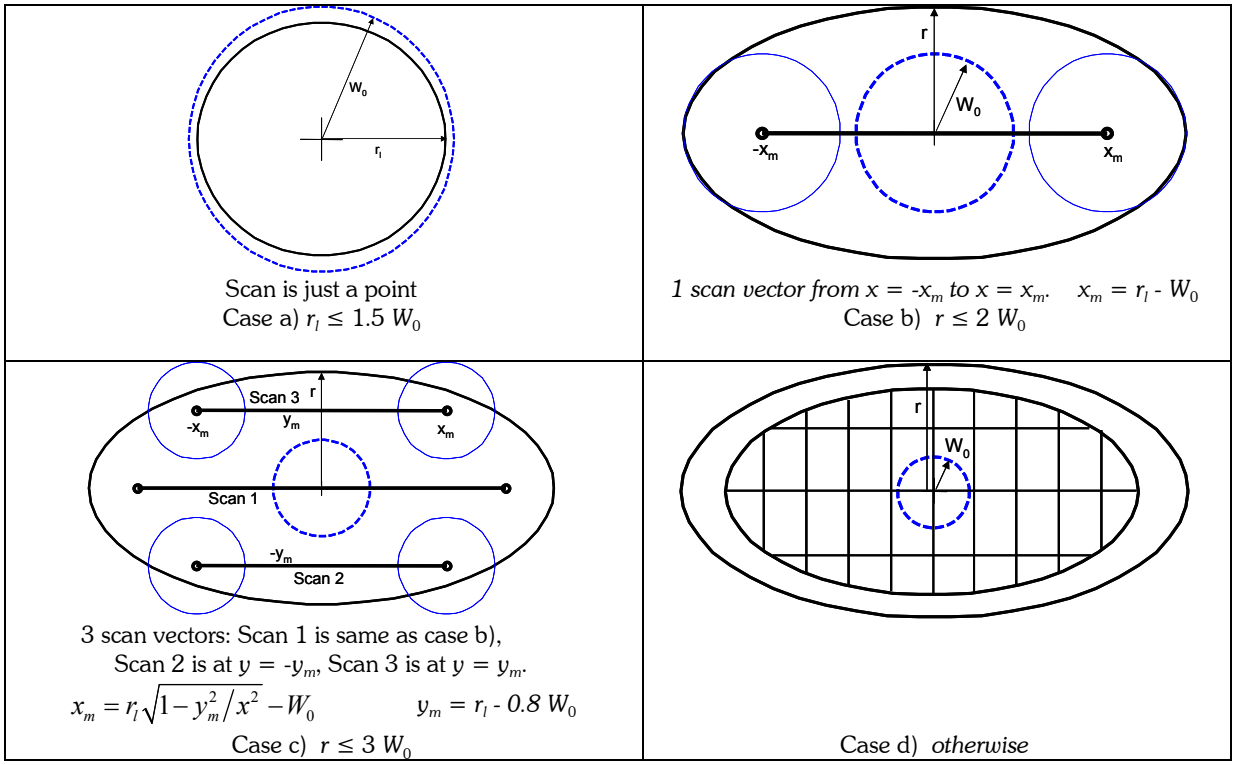

Fig. 5: Scan pattern cases for sliced struts.

Substituting reasonable values for a SLA-250/50 machine (P_L = 30 mW, W_0 = 0.125 mm, E_c = 0.12 mJ/mm2, l = 0.1mm, D_p = 0.1524 mm) yields a scan speed of about 600 mm/s. At this speed, the width of a cured scan line is 0.172 mm for the numbers in this example, or about 2/3 of the laser beam diameter. The cure model presented briefly here has been implemented into a MEL for lattice unit cells fabricated using SL. By adjusting scan speeds, it is possible to fine-tune a process plan such that lattice struts have appropriate sizes, which has been formulated as a parameter estimation problem and solved using nonlinear least-squares methods [12].

3.4 Process Planning

Process planning is denoted by the mapping $\Phi^{-1} : S \rightarrow P$. Using the notation in Fig. 3, process planning consists of two parts, one dealing with geometry decomposition ($\Phi^{-1} : S_G \rightarrow P_G$) and the other for assigning values to process variables ($\Phi^{-1} : S_M \rightarrow P_M$) to process the material appropriately. The specifics of the geometric decomposition and process modeling were covered in Section 3.3. In this section, we will briefly present the process planning formulation. Parameter estimation, or "inverse design," methods can be applied to AM process planning to enable plans to be designed that meet design requirements on shape, surface finish, tolerances, and potentially other properties such as stiffness. Inverse design methods were developed in the heat transfer area [9]. A typical application of inverse design methods is to layout heater elements in a furnace, where heater positions are to be adjusted to achieve a desired temperature distribution. Parameter estimation methods for SL will be used to achieve a desired surface finish. The surfaces of a part fabricated in SL are defined by where the resin reaches a high enough crosslink density to remain solid, which is related to the exposure received from the laser [6]. The challenge is to determine appropriate exposure levels for each laser scan as it draws part cross sections such that part surfaces are precisely positioned and shaped.

The inverse design problem for SL process planning can be stated as: **find** exposure values along each scan vector to **minimize** the deviation of exposure across part surfaces from the desired constant E_c value. A general mathematical problem formulation is shown in Fig. 6 [12]. The constraint models the height of the part at a point P on its surface, which has to be equal to the summation of the layer thicknesses at point P and the thickness of the Compensation Zone at point P. The objective function to be minimized models the deviation of exposure at a set of grid points (on the part's down-facing surfaces) from the critical exposure, E_c.

Since there are many more scan vectors than measurement points m_j, least-squares solution techniques are appropriate. We can take advantage of the MEL model by utilizing MEL parameterizations to sample each MEL and to compute exposure values. The least-squares fitting problem can be formulated as follows. The squared error term is the square of the objective function from Fig. 6, denoted by D (Eqn. 3). This error term is to be minimized, so the derivative of D, with respect to the vector of variables U, involves the Jacobian of the system. Since **J** is nonlinear, an iterative solution technique must be used to solve for the unknowns, which are the scanning velocities and some scan vector positions. Both Gauss-Newton and Levenburg-Marquardt methods [10] are frequently used to solve such problems. In our work, we use Matlab's non-linear least-squares solver, lsqnonlin, which selects from Gauss-Newton and Levenburg-Marquardt algorithms to solve problems.

Given: Geometry of the part $g(x,y,z)$
Material properties: energy absorption, α, critical exposure, E_c.

Find: LT_i, OC_{ip}, CZ_p

Satisfy:

Constraints: $h_p = \sum_{i=1}^{n} LT_i + CZ_p$

Bounds: on variables

Minimize: $\sum_{i=1}^{n} e^{\alpha(LT_i + OC_{ip})} e^{-\alpha\left[\sum_{m=1}^{i} LT_m + CZ_p\right]} - 1$ for all grid points P

Fig. 6: Math formulation of general process planning problem.

4. EXAMPLE

As an example, a cover plate for an aerospace structure will be redesigned to use lattice structure to stiffen it. The cover plate is shown in Fig. 7. It is approximately 300x350 mm in size and 3 mm thick. The thickness will be increased to 9 mm to accommodate the lattice structure, while the skin thickness will be decreased to 1.5 mm. A typical design-manufacture scenario will be presented that includes the decomposition of the cover plate geometry into cells, the synthesis of the resulting cellular structure to achieve a desired stiffness with minimum weight, and the decomposition of the synthesized geometry into manufacturing operations using MELs. The central region of the plate, inside of the bolt hole pattern, is offset by the desired thickness of the lattice structure. This central region is then decomposed into lattice cells by mapping one layer of octet truss cells into the region. A nominal size of 8x8x8 mm is chosen for the cells, which

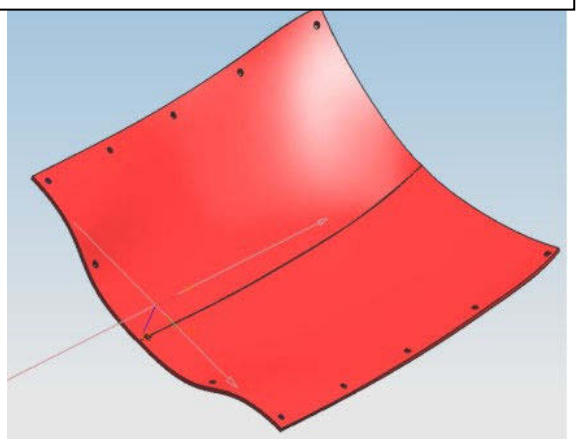

Fig. 7: Cover plate example part.

results in 14,960 struts.

To achieve the objectives of a target stiffness (modeled by a target deflection) and minimum weight, a shape optimization problem is solved. Lattice strut diameters are the design variables. Rather than allowing each of the strut diameters to be a variable, we adopt the strategy of grouping struts into clusters based on an initial structural analysis. Ten clusters were used, corresponding to 10 design variables for optimization, since in our experience good results are often achieved. Diameter variables can vary between 0.2 and 1.2 mm, corresponding to the minimum manufacturable strut size on the lower end. A reasonably large strut size is chosen for the maximum of the range; if the strut diameters become larger, the cells start to lose porosity. The loading condition for size optimization is an area load in the plate center of 0.064 N/mm^2 applied to a 60x60 mm area.

Size optimization is performed in ANSYS. Input files are automatically generated for ANSYS from the cellular model. The first-order gradient optimization method is used. Results are shown in Tab. 1. The number of optimization iterations, maximum stress, maximum deflection of the cover plate, and part volume are reported, along with the values of the diameter variables. This problem was not sensitive to the number of clusters used. Convergence of the cluster diameters was smooth, with the lower stress clusters becoming thicker, some mid-level clusters fluctuating up or down, as shown in Tab. 1. The final cover plate design is shown in Fig. 8. Note that various strut diameters can be seen in the zoomed view.

Diameters	**Initial [mm]**	**Final [mm]**		**Initial [N/mm^2]**	**Final [N/mm^2]**
D1	0.2	0.2	**Max. Stress**	-278.15	57.33
D2	0.4	0.6			
D3	0.6	0.79	**Volume**	**Initial [mm^3]**	**Final [mm^3]**
D4	0.6	0.73		8008	20,314
D5	0.8	0.84			
D6	0.8	0.73			
D7	1.0	0.88			
D8	1.0	1.04			
D9	1.2	1.2			
D10	1.2	1.2			

Tab. 1: Lattice optimization results.

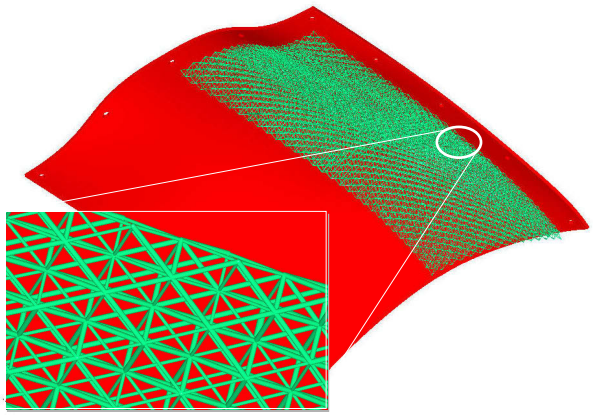

Fig. 8: Cover plate with optimized lattice structure (shown on only half of the plate).

The next step in the DFAM process is process planning to ensure manufacturability. Each unit cell of the lattice structure is represented by a lattice MEL from Section 3.3. Recall that the relative orientation of each strut to the build direction dictates how it will be decomposed into manufacturing operations, which, in the case of SL or SLS are laser scans. Each strut is modeled as a MEL to facilitate process planning and process simulation. The strut design from Fig. 9 is decomposed into MELs and process planning is performed. Of the many struts in the design, we will illustrate the process planning of only two of them. First, a low stress strut near the lower left-hand corner of the lattice will be examined; second a strut with a very high stress will be planned so that its lower surface is as smooth as possible to avoid stress concentrations.

The first strut is 0.2 mm in diameter and is bounded by nodes at (0,-146, 0.0745) and (4, -146, 0.274). The strut has the smallest allowable diameter since it was in the lowest stress category. Assume that the part will be built on a SLA-250/50 machine with a laser beam radius of W_0 = 0.125 mm. This situation corresponds to a Case (a) MEL, since $r_l \leq 1.5\ W_0$. The strut is at an angle of only 1.389 degrees with respect to the horizontal. It crosses only a few layers. Following the process plan method of Case a, the process plan consists of a total of 12 vector scans on only 4 layers. The SLA-250/50 has a top scan speed of about 1500 mm/sec, so is limited in its capability to fabricate thin struts. A layer thickness of 0.1 mm was used. Fig. 9 shows this part and its process plan. The scan vectors are shown as thin black lines terminated with circles; they are also labeled. The desired strut profile is shown using dotted red lines, while the resulting as-manufactured strut profile is shown as the thick blue lines.

After process planning, the scan speeds for the 12 scan vectors were computed as follows: V_1 = 1000 mm/s, V_2 = 1034 mm/s, V_3 = 682 mm/s, and V_4 through V_{12} were all the maximum speed, 1500 mm/s. As is evident, only the first three scans were at speeds other than the laser's top speed. Only in the vicinity of the left side of the strut are the

thicknesses such that slower speeds are needed. Otherwise, the laser scans at its top speed, which is not fast enough to fabricate the thin strut sections desired. The as-manufactured shape differs significantly from the desired strut shape, but this is to be expected given the machine's limitations. However, the strut is very thin and only lightly loaded, so small manufacturing errors such as this are insignificant.
For the sake of illustration, the presentation here focused on the body of the strut, not the nodes at its end-points. Three to eight struts are incident at nodes, so the process planning of the nodes is more complicated.

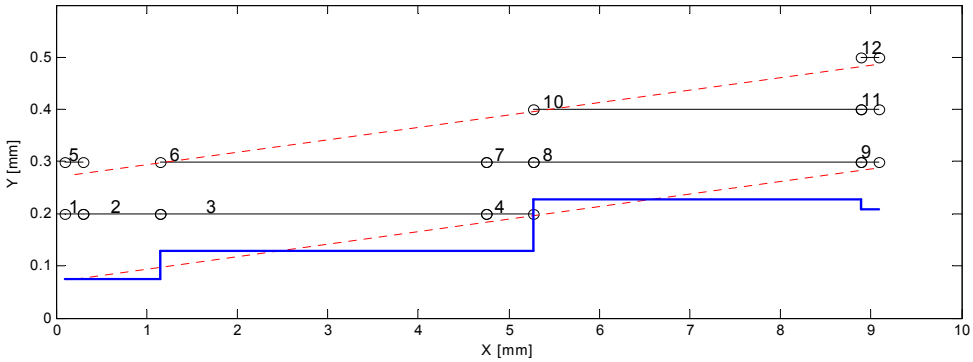

Fig. 9: Process plan for flat strut.

The second strut to be investigated as a highly loaded strut near the center of the part; its coordinates were (200, 0, 37.44) and (200, -6.33, 33.38). It is 7.52 mm long, 1.2 mm in diameter, and at an angle of 32.68 degrees to the horizontal. Since it is highly loaded, it was in category 10 and had the largest allowable diameter.
Process planning was based on a Case (d) MEL, with a default scan pattern. In this case, only scans in the transverse direction (X coordinate direction) were used. Fig. 10 shows the process plan, where each '*' denotes a laser scan. The layers are clearly evident. The blue lines and asterisks denote part geometry, while the red circles indicate points along the geometry where laser exposure was measured. The pink rectangle at the bottom indicates support structure (added automatically by the process planning tool, but not actually built for individual struts). The parameter estimation method described in Section 3.4 was used for process planning. After planning, the strut manufacturing plan was simulated and resulted in the strut profile shown in Fig. 11. Note that the bottom profile is much smoother than the top surface and indicates the capability of our process planning method. The profile of the strut top is defined by the layers used in the SL process (0.1 mm layer thickness).

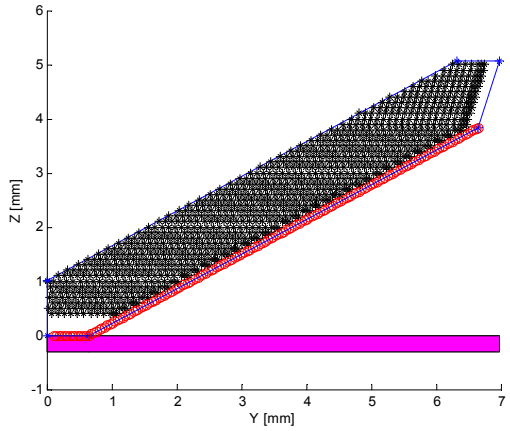

Fig. 10: Process plan for high stress strut.

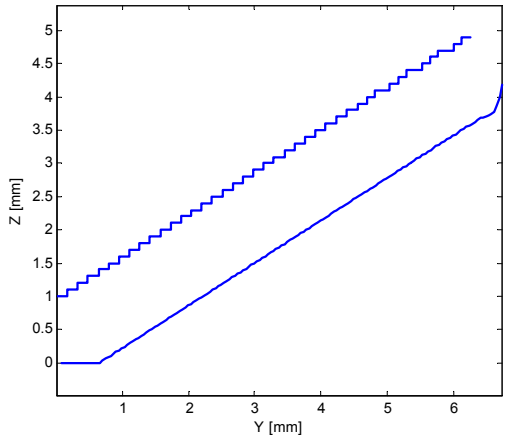

Fig. 11: Profile of as-manufactured strut.

5. CONCLUSIONS

Two advances are reported in this paper. First, a new Design for Additive Manufacturing (DFAM) method was presented that supports part and specification modeling, process planning, and manufacturing simulations. Second,

Manufacturable ELements (MELs) were proposed as an intermediate representation for supporting the manufacturing related aspects of the method. Specific conclusions from this work include:

- Cellular material types provide one method for providing mesostructure within a part for achieving improved stiffness, strength, or other functional requirements, as compared to monolithic materials.
- Non-manifold modeling provides a useful abstraction for representing some cellular mesostructures so that full 3D solid modeling is not necessary when thousands of shape elements are present in a design.
- Manufacturing ELements (MELs) enable process planning within discrete regions of a part and also enable process simulation. MELs represent one approach to achieving shape-specific process planning, rather than a reliance on general purpose process planning methods, typical of the AM industry at present.
- Design for Additive Manufacturing should be concerned with the exploration of expanded design spaces, rather than the focus on constraints imposed by the manufacturing processes, as is typical of DFM methods.

6. ACKNOWLEDGEMENTS

We gratefully acknowledge the U.S. National Science Foundation, through grants IIS-0120663 and DMI-0522382, and the support of the Georgia Tech Rapid Prototyping and Manufacturing Institute member companies, particularly Pratt & Whitney, for sponsoring this work.

7. REFERENCES

[1] Ashby, M. F.; Evans, A.; Fleck, N. A.; Gibson, L. J.; Hutchinson, J. W.; and Wadley, H. N. G.: Metal Foams: A Design Guide, Butterworth-Heinemann, Woburn, MA, 2000.

[2] Deshpande, V. S.; Fleck, N. A.; Ashby M. F.: Effective Properties of the Octet-Truss Lattice Material, Journal of the Mechanics and Physics of Solids, 49(8), 2001, 1747-1769.

[3] Ensz, M.; Storti, D.; Ganter, M.: Implicit Methods for Geometry Creation, International Journal of Computational Geometry Applications, 8(5,6), 1998, 509–36.

[4] Gibson, L. J.; Ashby, M. F.: Cellular Solids: Structure and Properties, Cambridge University Press, Cambridge, UK, 1997.

[5] Gursoz, E. L.; Choi, Y.; Prinz, F. B.: Vertex-based Representations of Non-manifold Boundaries, Geometric Modeling for Product Engineering, IFIP WG5.2, Rensselaerville, NY, M. J. Wozny, J. U. Turner, and K. Preiss, (eds.), North-Holland, Amsterdam, 1988, 107-130.

[6] Jacobs, P. F.: Rapid Prototyping & Manufacturing, Fundamentals of Stereolithography, SME, Dearborn, MI, 1992.

[7] Johnston, S. R.; Reed, M.; Wang, H.; Rosen, D. W.: Analysis of Mesostructure Unit Cells Comprised of Octet-truss Structures, Solid Freeform Fabrication Symposium, Austin, TX, Aug. 14-16, 2006, 421-432.

[8] Olson, G. B., Computational Design of Hierarchically Structured Materials, Science, 277(5330), 1997, 1237-1242.

[9] Özisik, M. N.; Orlande, H. R. B.: Inverse Heat Transfer, Taylor & Francis, New York, 2000.

[10] Press, W. H.; Teukolsky, S. A.; Vettering, W. T.; Flannery, B. P.: Numerical Recipes in C, Chapter 15, 2nd Edition, Cambridge University Press, Cambridge, UK, 1992.

[11] Rosen, D. W.; Atwood, C.; Beaman, J.; Bourell, D.; Bergman, T.; Hollister, S.: Results of WTEC Additive/Subtractive Manufacturing Study of European Research, Proc. SME Rapid Prototyping & Manufacturing Conference, paper # TP04PUB211, Dearborn, MI, May 10-13, 2004. Also, see: http://wtec.org/additive/welcome.htm for the complete report.

[12] Sager, B.; Rosen, D. W.: Use of Parameter Estimation For Stereolithography Surface Finish Improvement, Proc. Solid Freeform Fabrication Symposium, Austin, TX, Aug. 1-3, 2005.

[13] Shapiro, V.; Tsukanov, I.: Meshfree Simulation of Deforming Domains, Computer-Aided Design, 31(7), 1999, 459-471.

[14] Wang, H.; Chen, Y.; Rosen, D. W.: A Hybrid Geometric Modeling Method for Large Scale Conformal Cellular Structures, Proc. ASME Computers and Information in Engineering Conference, paper DETC2005-85366, Long Beach, CA, Sept 24-28, 2005.

[15] Wang, H.; Rosen, D. W.: Parametric Modeling Method for Truss Structures, ASME Computers and Information in Engineering Conference, paper DETC2002/CIE-34495, Montreal, Sept. 29-Oct 2, 2002.

[16] Wang, A.-J.; McDowell, D. L.: Optimization of a metal honeycomb sandwich beam-bar subjected to torsion and bending, International Journal of Solids and Structures, 40(9), 2003, 2085-2099.